


# Room-temperature Magnetoresistance in Hybrid Halide Perovskites: Effect of Spin-Orbit Coupling

Arnab Banerjee\* and Goutam Paul

*School of Physical Sciences, Indian Association for the Cultivation of Science, Jadavpur, Kolkata-700032, India*

 (Received 30 June 2020; revised 6 September 2020; accepted 11 November 2020; published 4 December 2020)

Hybrid halide perovskites have emerged as promising materials for spintronics research due to their significant and tunable spin-orbit coupling (SOC). However, experimental findings that can discern the correlation between spintronic properties and SOC are rare. Here, we report the observation of room-temperature magnetoresistance (MR) and discuss the influence of chemical modification, hence SOC, in lead-based hybrid halide perovskites. Suppression of current under magnetic field ( $B$ ) in perovskite thin films is explained in terms of field-modulated spin-mixing activity. We find that the MR increases upon replacement of  $I^-$  with  $Br^-$  and  $Cl^-$ . The internal magnetic field parameter, i.e., HWHM of  $MR(B)$  reduces as we replace  $I^-$  by  $Br^-$  and  $Cl^-$  evidencing SOC is indeed weakened on substituting  $I^-$  with lighter halogen ions. Moreover, we analyze the effect of organic cation exchange by replacing  $MA^+$  with  $FA^+$  but no drastic change in MR response is observed. Our results successfully establish the crucial role played by SOC on MR for the development of spintronic devices, based on hybrid halide perovskites.

DOI: [10.1103/PhysRevApplied.14.064018](https://doi.org/10.1103/PhysRevApplied.14.064018)

## I. INTRODUCTION

A rather unusual and comparatively less explored aspect of hybrid halide perovskites is their potential use in spintronic applications. Apart from their extraordinary optoelectronic properties [1], such as the emission of strong photoluminescence [2], a high extinction coefficient in the visible wavelength region [3], tunable band gap [4], a low exciton binding energy for efficient charge separation [5], long carrier diffusion length [6], a high [7] and ambipolar carrier mobility [8] due to smaller electron and hole effective masses, their spintronic properties have also attracted immense interest from the scientific community. Furthermore, properties like solution-processed growth [9] and broad tuning of chemical composition in the perovskite structure [10] make them beneficial particularly for spintronics.

The magnetoresistance (MR) effect of a material refers to the propensity of changing its electrical resistance upon application of an external magnetic field. MR can generally be observed under the spin-valve geometry when the parallel and antiparallel arrangement of the outermost ferromagnetic electrodes, having different coercive fields, could be achieved by swiping an externally applied magnetic field [11,12]. Besides, in the case of nonmagnetic semiconductors spin blockade, scattering of conduction electrons by defects and disorder could be the possible origin of MR [13–15]. However, electroluminescence studies

in hybrid halide perovskites have revealed that an external magnetic field can change the electrical injection current in light-emitting diodes under non-spin-polarized charge injection [16]. These sorts of magnetic field effects are intrinsic to the perovskites and successfully explained by the “ $\Delta g$  mechanism” [16,17] (where  $\Delta g$  is the difference between the  $g$  factor of the electron and hole in the spin-pair species) regardless of the limitations imposed by strong spin-orbit coupling (SOC) [18,19].

The presence of heavy atoms, such as lead (Pb) in their chemical composition induces a notable SOC, affecting the electronic band structure of the particular class of materials [20]. Even in the case of bulk centrosymmetric materials, defects arising out of the interfaces, surfaces, and grain boundaries locally break the inversion symmetry [21]. Consequently, SOC strength in conjunction with the breaking of inversion symmetry, immediately leads to unique spin-dependent properties [22,23]. In addition, room-temperature ferromagnetism [24], moderate spin lifetime, and reasonably large spin diffusion length makes it usable as a promising material for spintronic application [25–27]. To date, spin-related phenomena such as light-induced magnetic switch [28], magnetic field effects [16], spin-selective optical Stark effect [29,30], and also Rashba spin splitting [31,32] have been demonstrated in hybrid halide perovskites both from the theoretical and experimental point of view. Although few works have taken place [33,34], a proper understanding of the phenomena governing the ordinary MR effect in pristine hybrid halide-perovskite systems is still insufficient.

\*sspab5@iacs.res.in

In this work, we study the room-temperature MR effect in electrical injection current of Pb-based hybrid halide perovskites having  $\text{APbX}_3$  structure, where A and X represents monovalent organic cation and halogen anion, respectively. Moreover, we vary the inorganic halide ions and organic cations that enable a synthetic tuning of SOC. Hence, our result is likely to provide useful information on the occurrence of MR, as well as the rationale behind the effect of SOC on MR in these hybrid halide-perovskite systems. Undoubtedly, addressing the underlying mechanism of MR can impact on the magnetic field control of the electronic properties of perovskites in magnetic devices, paving the way towards spintronics-related applications with these classes of fascinating materials.

## II. MAGNETORESISTANCE IN HYBRID PEROVSKITE THIN FILMS

The thin films and devices based on lead halide perovskite having different halogen (iodine, bromine, and chloride) and organic cation (methylammonium and formamidinium) are fabricated by following a standard technique [35] (see experimental details [36]). The characteristic absorption spectra of perovskites  $\text{MAPbI}_3$ ,  $\text{MAPbBr}_3$ ,  $\text{MAPbCl}_3$ , and  $\text{FAPbI}_3$  presented in Fig. 1(a) shows a strong absorption in visible wavelength range with optical band gaps 1.59, 2.3, 3.05, and 1.5 eV, respectively, as obtained from the Tauc plots (see Fig. S1 within the Supplemental Material) [36]. The x-ray diffraction (XRD) patterns presented in Fig. 1(b) show the distinct position of characteristic peaks for four different perovskites and these patterns match well with the reported results [37,38]. Thus, the optical absorption spectra along with the XRD pattern confirms the phase purity of these perovskites.

To investigate the effect of magnetic field ( $B$ ) on electrical conductivity of hybrid halide perovskites, the current ( $I$ )-voltage ( $V$ ) characteristics of  $\text{MAPbI}_3$  thin films are first recorded both in the presence and absence of  $B$  with strength approximately 400 mT at room temperature. A schematic of the device used in our study is presented in Fig. 1(c) where electrodes are chosen to facilitate carrier injection from the opposite electrodes. The active junction area of the device is approximately  $10 \text{ mm}^2$ . We intentionally apply external magnetic field,  $B$ , in a direction perpendicular to the sample surface. In Fig. 1(d),  $I$ - $V$  characteristics are nonlinear in nature and typical for the semiconducting active materials. The little asymmetry in the  $I$ - $V$  curve appears due to the inequality of the work functions of the two electrodes. From Fig. 1(d), a clear suppression in current value upon application of  $B$  can be observed, which indicates the presence of MR in  $\text{MAPbI}_3$ . Here MR is defined as

$$\frac{\Delta R}{R} = \frac{R(B \neq 0) - R(B = 0)}{R(B = 0)} = \frac{I(B = 0) - I(B \neq 0)}{I(B \neq 0)}, \quad (1)$$

where,  $R(B \neq 0)$ ,  $I(B \neq 0)$ , and  $R(B = 0)$ ,  $I(B = 0)$  are the resistances and current values at a fixed applied bias in the presence and absence of  $B$ , respectively. We obtain a positive MR as approximately 10% at 2.0 V for  $\text{MAPbI}_3$  as calculated from Eq. (1). We should note here that the MR values were obtained at the current values more than  $70 \mu\text{A}$ . So, to nullify the current-induced heating effects in the MR response, we measure the  $I$ - $V$  response in alternating sequences after switching *on* and *off* the magnetic field. Figure S2 within the Supplemental Material shows multiple measurements with and without magnetic fields, highlighting the absence of current-induced heating effects and the reproducible MR response as well [36].

Observation of MR effect in  $\text{MAPbI}_3$  thin film can be described on the basis of formation of correlated electron-hole ( $e^-h^+$ ) spin-pair species in the triplet ( $T_{m=+1} = |\uparrow\uparrow\rangle$ ,  $T_{m=-1} = |\downarrow\downarrow\rangle$ , and  $T_{m=0} = (|\uparrow\downarrow\rangle + |\downarrow\uparrow\rangle)/\sqrt{2}$ ) and singlet ( $S_{m=0} = (|\uparrow\downarrow\rangle - |\downarrow\uparrow\rangle)/\sqrt{2}$ ) configurations; and modulation of their population under external magnetic field. We note that small spin-lattice relaxation time of the spin-pair species in  $\text{MAPbI}_3$  due to strong SOC-imposed restrictions in exhibiting MR [18,19]. But, the nontrivial  $\Delta g$  in a spin-pair species [39] could lead to the observable MR.

Assuming a spin-independent electron-hole capture process (as innate in the Langevin model), the spin-correlated  $e^-h^+$  pair gets created when electrons and holes from opposite electrodes approach each other under the influence of electric field having an initial singlet-to-triplet ratio 1:3 [40]. Due to small exchange interaction [39], emanating from the organic cation-induced  $e^-h^+$  charge separation, the four spin-paired levels are equally populated at room temperature reaching the steady state. That is, in the absence of  $B$ , the constant competition between SOC strength, leading to spin mixing, and the exchange correlation, which is responsible for spin conservation, in the singlet and threefold degenerate triplet states results in a state of dynamic equilibrium [41,42]. Due to the complicated recombination based on the spin-selection rule, the spin-correlated  $e^-h^+$  pair in its triplet configurations, which are more prone to dissociate into free carriers, gives rise to steady-state current. But the application of  $B$  can perturb this equilibrium by modulating the singlet and triplet steady-state populations.

When  $B$  is applied, the coherent relationship between the electron and hole precessions starts to be destroyed due to the field-induced additional precession for the  $e^-h^+$  pair during electron and hole recombination [43]. Additionally,

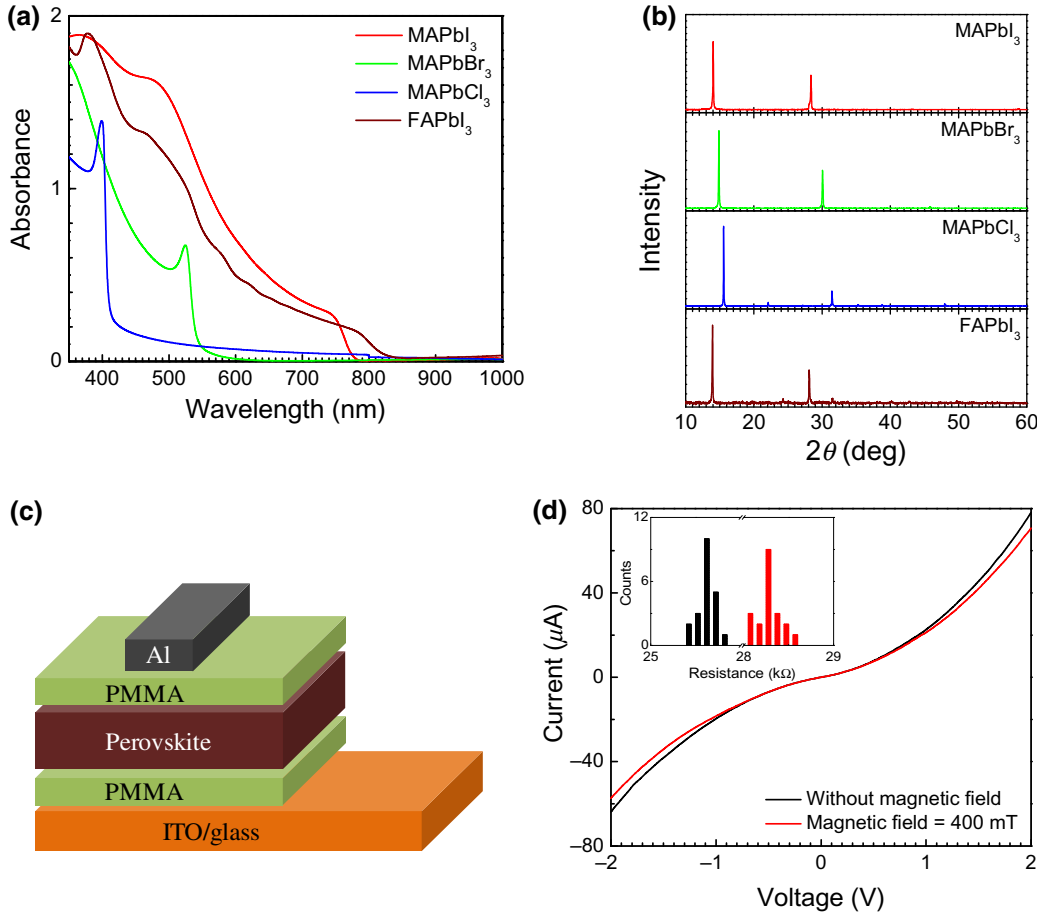


FIG. 1. (a) Absorption spectra and (b) XRD patterns of MAPbI<sub>3</sub>, MAPbBr<sub>3</sub>, MAPbCl<sub>3</sub>, and FAPbI<sub>3</sub> on glass substrate. (c) Schematic device structure and (d) current-voltage characteristics of ITO/PMMA/MAPbI<sub>3</sub>/PMMA/Al heterojunction with (red curve) and without (black curve) 400-mT applied magnetic field. Inset showing the representative resistance histograms of the said junction with (red) and without (black) applied 400-mT magnetic field depicting MR.

in the case of MAPbI<sub>3</sub>, owing to a high  $\Delta g$  value (which is more than 2 orders of magnitude higher than the ordinary organic semiconductors) [44,45], a sufficient amount of spin mixing between singlet and triplet could occur at a rate ( $\Delta\omega_p$ ):

$$\Delta\omega_p = \mu_B \Delta g B / \hbar, \quad (2)$$

where  $\mu_B$  is the Bohr magneton and  $\hbar$  is the reduced Planck constant. So, the rate of transfer between singlet and triplet increases with magnetic field. Consequently, the different spin-pair dissociation rate for singlet and triplets [46] leads to a variation in the steady-state conductivity with  $B$ . Figure 2 schematically depicts the mechanism of MR response.

To be precise, under the influence of  $B$ , spin mixing between singlet ( $S_{m=0}$ ) and only  $T_{m=0}$  triplet level occurs rather than the singlet with whole triplet manifolds. Thereby the spin characteristic of each component of this mixed state is dependent on  $B$ . So, in the presence of  $B$ , a lesser fraction of  $e^-h^+$  pairs available for dissociation in the triplet configuration. In contrast, when  $B$  is not applied, the fraction of  $e^-h^+$  pairs in triplet configuration is higher due to intermixing of all available states (than in the case of intermixing only between  $S_{m=0}$  and  $T_{m=0}$  states). So

in the presence of  $B$ , current resulting from the dissociation of triplet spin-pair species into free carriers decreases. Consequently, we observe a positive MR.

### III. EXPLORING THE EFFECTS OF SOC ON MR IN PEROVSKITES

We can admit that the hybrid halide perovskites possess a strong SOC due to the presence of heavy elements like Pb [47]. On the experimental side, it has been shown that spintronic properties can be tuned by changing the elemental composition of the perovskites supporting the relevant change in SOC strength [26]. Hence, our strategy is to track the MR response by performing targeted chemical substitutions, such as halide substitution and cation exchange within the Pb-based hybrid halide-perovskite framework.

#### A. Effect of halide modification

We accordingly compare the  $I$ - $V$  responses for MAPbBr<sub>3</sub> and MAPbCl<sub>3</sub> thin films by applying an external field of approximately 400 mT at an applied bias of 2.0 V [see Figs. 3(a) and 3(b)] with MAPbI<sub>3</sub>. Such characteristics at different field strengths with MAPbI<sub>3</sub>, MAPbBr<sub>3</sub>, and MAPbCl<sub>3</sub> as active perovskite layers are collated in

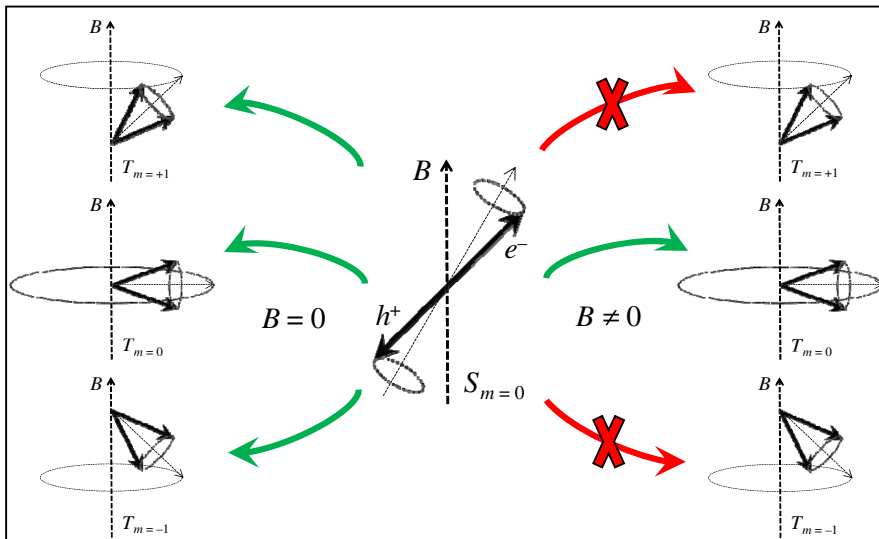


FIG. 2. Schematic representation of the mechanism behind the origin of MR in hybrid halide perovskites. While the left panel shows the response in the absence of  $B$ , the right panel presents the case in the presence of external  $B$ .

Figs. S3, S4, and S5 within the Supplemental Material, respectively [36]. As we can see, the relative suppression in magnitude of current after applying  $B$  is much higher in the case of MAPbCl<sub>3</sub> than the others, leading to higher

MR in MAPbCl<sub>3</sub> compared to MAPbI<sub>3</sub> and MAPbBr<sub>3</sub>. We should note here that Cl<sup>-</sup>, Br<sup>-</sup>, and I<sup>-</sup> are three different halide ions with gradually increasing atomic numbers ( $Z$ ) of 17, 35, and 53, respectively. Consequently, they yield

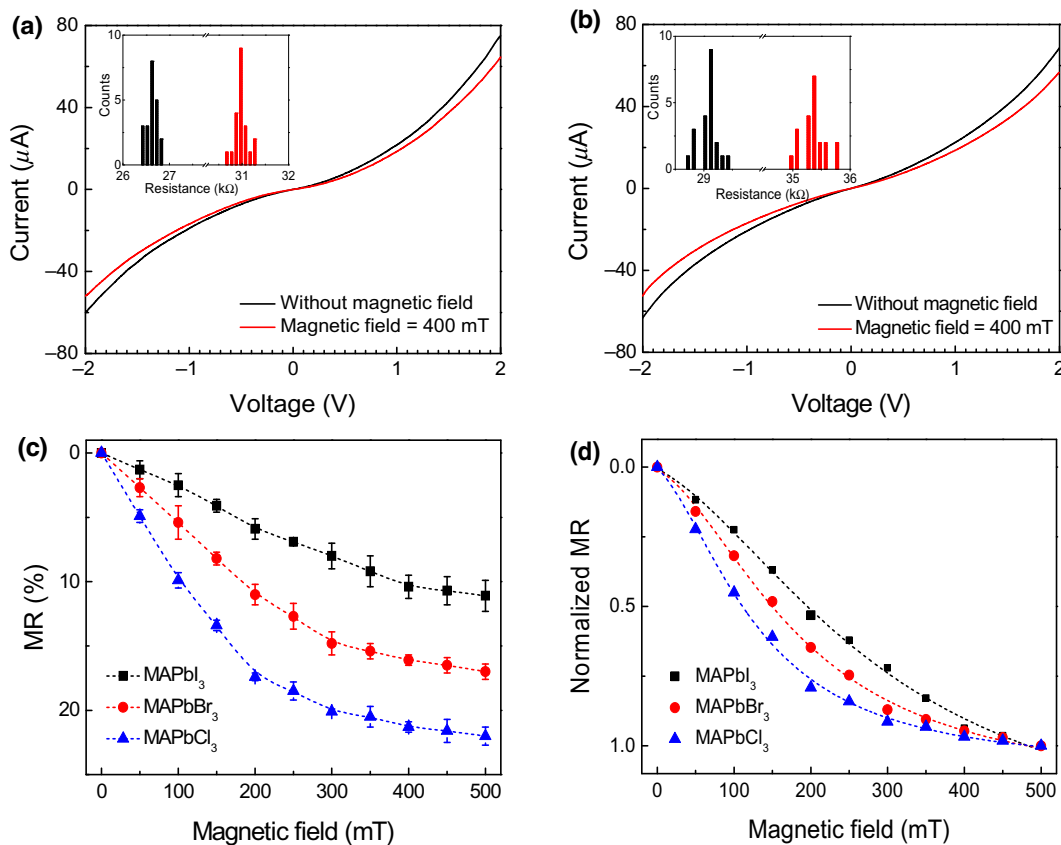


FIG. 3. Current-voltage characteristics of (a) ITO/PMMA/MAPbBr<sub>3</sub>/PMMA/Al and (b) ITO/PMMA/MAPbCl<sub>3</sub>/PMMA/Al heterojunctions with (red curve) and without (black curve) 400-mT applied magnetic field. Inset showing the representative resistance histograms of the said junction with (red) and without (black) applied 400-mT magnetic field depicting MR. (c) MR response of MAPbI<sub>3</sub> (black), MAPbBr<sub>3</sub> (red), and MAPbCl<sub>3</sub> (blue). (d) Dotted curve represents the Lorentzian fitting of normalized MR response [color code the same as in (c)].

a difference in SOC parameter that scales with  $Z^4$ . This is manifested in the increment of MR of MAPbCl<sub>3</sub> compared to MAPbBr<sub>3</sub> and MAPbI<sub>3</sub> suggesting a strong influence of SOC.

To get further insight on the observed difference in MR response, we further compare the MR response in these three perovskite systems by varying the magnetic field,  $MR(B)$ . In Fig. 3(c), it can be observed that applying a magnetic field causes a positive MR in each device along with the increment in magnitude of MR upon increase in  $B$ . More importantly, the change is sharper in the case of MAPbCl<sub>3</sub> than the other hybrid perovskites containing Br<sup>-</sup> and I<sup>-</sup>. Now to check the sharpness of change of the  $MR(B)$  response, we perform a curve fitting of the normalized MR based on Lorentzian function [48] and from the HWHM we determine the internal magnetic parameter ( $B_{1/2}$ ) correlated to the SOC strength. From Fig. 3(d), we determine  $B_{1/2} \sim 320$  mT,  $B_{1/2} \sim 201$  mT, and  $B_{1/2} \sim 143$  mT for iodide, bromide, and chloride-based perovskites, respectively, denoting a larger line shape broadening in the case of MAPbI<sub>3</sub>.

To comment on the observed change, it is necessary to recall the rate of change of the singlet-to-triplet ratio ( $\chi$ ) in the presence of magnetic field (which is denoted by  $\partial\chi/\partial B$ ). As the SOC parameter decreases, it is easier for external magnetic field to destroy the population equilibrium between singlet and triplet states. So, as the

equilibrium becomes weaker,  $\partial\chi/\partial B$  increases; this causes a narrower line shape of the  $MR(B)$ . This is evidenced from the gradual decrement in the line shape while changing the halide ions from I<sup>-</sup> to Cl<sup>-</sup> via Br<sup>-</sup>.

## B. Influence of cation exchange

Now, to explore the influence of cation exchange on MR in perovskites, we consider the FA equivalent of MAPbI<sub>3</sub>, FAPbI<sub>3</sub>. From previous studies, it can be reiterated that, cation-induced structural change endorsed markedly different electronic and optical properties in organohalide lead perovskites mediated by the different SOC strengths [49].

In Fig 4(a), we present the  $I$ - $V$  characteristics of FAPbI<sub>3</sub> thin films with and without 400-mT field and compare [in Fig. 4(b)] the  $MR(B)$  response between FAPbI<sub>3</sub> and MAPbI<sub>3</sub>. Remaining  $I$ - $V$  curves with different  $B$  are imprinted in Fig. S6 within the Supplemental Material [36]. While comparing the  $MR(B)$  of FAPbI<sub>3</sub> with MAPbI<sub>3</sub>, we do not observe any significant difference apart from a small reduction in MR magnitude. The observed behavior in MR response stems from the fact that there is an increment in the spin-orbit interaction in FAPbI<sub>3</sub>. It is predicted that an enhancement of SOC can occur on account of the cation-induced structural-phase transition [49]. Upon incorporation of FA<sup>+</sup>, pseudocubic structures of FAPbI<sub>3</sub> support an enhanced SOC compared

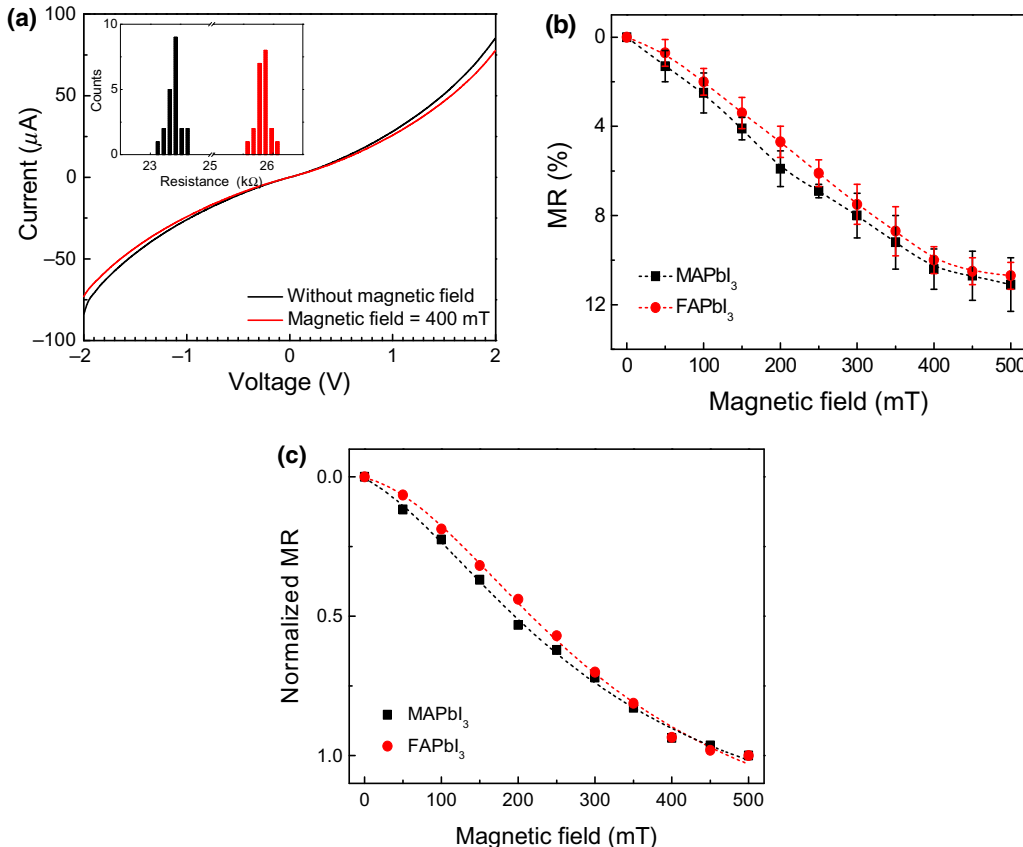


FIG. 4. (a) Current-voltage characteristics of ITO/PMMA/FAPbI<sub>3</sub>/PMMA/Al heterojunction with (red curve) and without (black curve) 400-mT applied magnetic field. Inset showing the representative resistance histograms of the said junction with (red) and without (black) applied 400-mT magnetic field depicting MR. (b) MR response of MAPbI<sub>3</sub> (black) and FAPbI<sub>3</sub> (red). (c) Dotted curve represents the Lorentzian fitting of normalized MR response [color code same as in (b)].



to octahedrally tilted tetragonal structures like MAPbI<sub>3</sub>. Since the ionic character is higher for Pb—I bonds in FAPI<sub>3</sub>, the Pb contribution in forming the conduction band increases, resulting in slightly higher SOC. From Fig. 4(c), we also quantify the half-width at half maxima to estimate the internal field parameter ( $B_{1/2}$ ). For FAPbI<sub>3</sub> it is  $B_{1/2} = \sim 329$  mT, which is higher than MAPbI<sub>3</sub> suggestive of a larger SOC.

### C. Discussions on spintronic properties

According to the “ $\Delta g$  mechanism,”  $B_{1/2}$  is related to spin lifetime ( $\tau$ ) as

$$\tau = \hbar / (2\mu_B \Delta g B_{1/2}). \quad (3)$$

We then calculate the  $\tau$  from the  $B_{1/2}$  values obtained from the observed MR( $B$ ) response. Here, we assume that the value of  $\Delta g$ , which varies as approximately  $(Z/137)^2$ , is 1 because of the presence of heavy elements (like Pb, I etc.) in perovskite structures. If we closely look at Table I, we notice two interesting things. First, as SOC increases while going downwards by column,  $\tau$  decreases. Secondly,  $\tau$  varies significantly upon changing the halide ions as compared to the organic cations. Consequently, we could find that the spintronic properties in hybrid halide perovskites are predominantly governed by the inorganic halide ions rather than the organic cations. This is in agreement with a current observation [26].

Apart from a report based on  $\tau$  measurement of single-crystal MAPbBr<sub>3</sub> [50], there are no other reports on  $\tau$  at room temperature. If we compare  $\tau$  for MAPbBr<sub>3</sub> thin film with that of the reported value, a smaller magnitude of  $\tau$  might be attributed to the higher degree of defects arising out of the grain boundaries in the case of solution-processed thin films. However, there are few works on measuring  $\tau$  at low temperatures [32,51]. Reduction in  $\tau$  compared to the low-temperature values can also be explained in terms of enhanced spin relaxation at room temperature [52]. Thus, the obtained values are particularly considerable.

While analyzing the MR across the hybrid halide-perovskite thin films, it is realized that as the amplitude of MR increases,  $B_{1/2}$  decreases implying a narrower MR( $B$ ). From the plot in Fig. 5(a), it can be seen that the normalized

TABLE I. Estimated spin lifetime ( $\tau$ ) using the  $\Delta g$  mechanism in hybrid halide perovskites.

Perovskite sample	MR <sub>max</sub> (%)	$B_{1/2}$ (mT)	$\tau$ (pS)
MAPbCl <sub>3</sub>	22.0	143	39
MAPbBr <sub>3</sub>	17.0	201	28
MAPbI <sub>3</sub>	11.1	320	18
FAPbI <sub>3</sub>	10.7	329	17

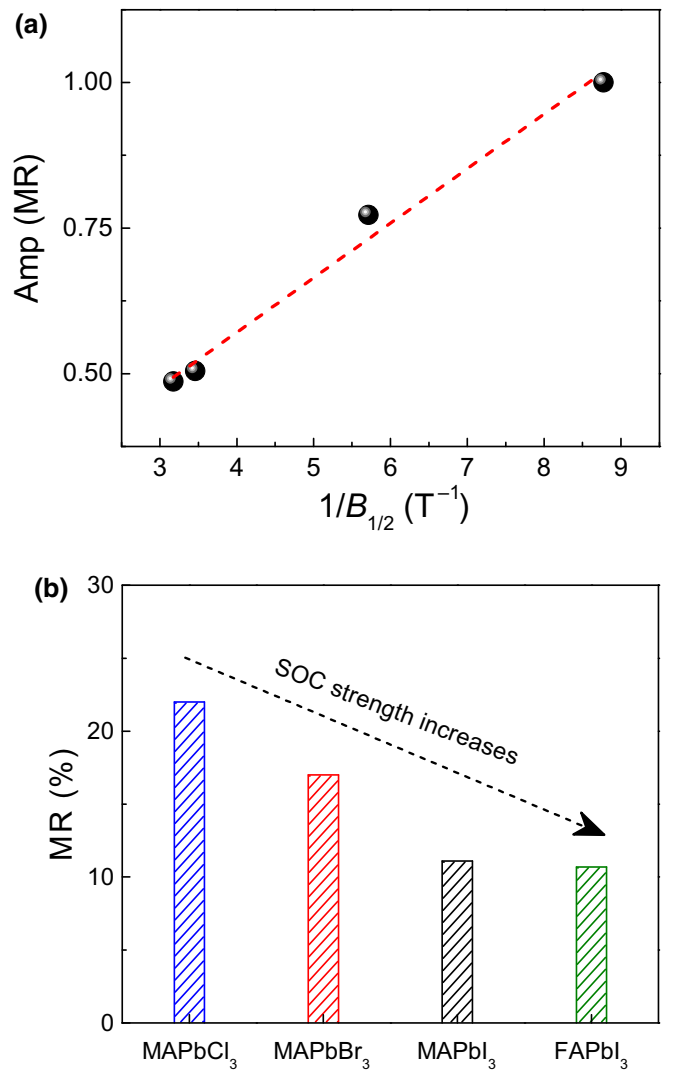


FIG. 5. (a) Variation of Amp(MR) with  $1/B_{1/2}$  and (b) effect of SOC on MR as compiled from Table I.

amplitude of MR, Amp(MR) depends linearly on the inverse of  $B_{1/2}$ . As a result, we can affirm that, this particular response of the Pb-based hybrid halide perovskites is an intrinsic property of this family of semiconductors and depends on an internal parameter, which is nothing but the SOC apart from varying arbitrarily among the thin films of different hybrid halide perovskites. Finally, in Fig. 5(b), we delineate the MR for the different perovskite films with comparable thickness depicting the fact that MR decreases as SOC increases. Moreover, MR in such cases could be dependent on the spin-dependent pair dissociation and/or recombination rates. Switching I<sup>-</sup> in MAPI<sub>3</sub> with lighter halogen atoms (Br<sup>-</sup> and Cl<sup>-</sup>), reduces the spin-orbit-interaction strength and increases MR magnitude. On the other hand, very minor reduction in MR is found while substituting MA by FA, lifting SOC strength.

#### IV. CONCLUSION

In conclusion, we report the observation of room-temperature MR in MAPI for magnetic fields up to 500 mT and describe this finding in terms of a spin-correlated  $e^-h^+$  pair and their occupation modulation in the spin-pair manifold under the action of  $B$ . Moreover, we find that the MR response becomes more prominent when we replace  $I^-$  with  $Cl^-$  ions in Pb-based hybrid halide perovskites. Our field-dependent MR plot indicates that when we substitute  $I^-$  with lighter halogen ions ( $Cl^-$ ,  $Br^-$ ) it reduces the internal magnetic field parameter ( $B_{1/2}$ ), providing direct evidence that SOC is indeed decreased in the bromide and chloride-based perovskites than in the case of iodide ones. Additionally, when we compare the MR( $B$ ) response by changing the organic cation from  $MA^+$  to  $FA^+$ , it also affects the amplitude of MR. In a nutshell, our results present an insightful understanding of the SOC effect in MR in hybrid halide-perovskite systems.

#### ACKNOWLEDGMENTS

A.B. acknowledges DST INSPIRE Fellowship No. IF 160121. G.P. acknowledges CSIR Fellowship No. 09/080(0958)/2014-EMR-I (Roll No. 521931). Authors also acknowledge Professor A.J. Pal of the Indian Association for the Cultivation of Science, Kolkata for providing the necessary support in performing the experiments.

- 
- [1] W. J. Yin, T. Shi, and Y. Yan, Unique properties of halide perovskites as possible origins of the superior solar cell performance, *Adv. Mater.* **26**, 4653 (2014).
- [2] F. Deschler, M. Price, S. Pathak, L. E. Klintberg, D.-D. Jarausch, R. Higler, S. Hüttner, T. Leijtens, S. D. Stranks, H. J. Snaith *et al.*, High photoluminescence efficiency and optically pumped lasing in solution-processed mixed halide perovskite semiconductors, *J. Phys. Chem. Lett.* **5**, 1421 (2014).
- [3] Y. Wang, S. Bai, L. Cheng, N. Wang, J. Wang, F. Gao, and W. Huang, High-efficiency flexible solar cells based on organometal halide perovskites, *Adv. Mater.* **28**, 4532 (2016).
- [4] S. A. Bretschneider, J. Weickert, J. A. Dorman, and L. Schmidt-Mende, Research update: Physical and electrical characteristics of lead halide perovskites for solar cell applications, *APL Mater.* **2**, 040701 (2014).
- [5] V. D’Innocenzo, G. Grancini, M. J. P. Alcocer, A. R. S. Kandada, S. D. Stranks, M. M. Lee, G. Lanzani, H. J. Snaith, and A. Petrozza, Excitons versus free charges in organo-lead tri-halide perovskites, *Nat. Commun.* **5**, 3586 (2014).
- [6] S. D. Stranks, G. E. Eperon, G. Grancini, C. Menelaou, M. J. P. Alcocer, T. Leijtens, L. M. Herz, A. Petrozza, and H. J. Snaith, Electron-hole diffusion lengths exceeding 1 micrometer in an organometal trihalide perovskite absorber, *Science* **342**, 341 (2013).
- [7] C. Wehrenfennig, G. E. Eperon, M. B. Johnston, H. J. Snaith, and L. M. Herz, High charge carrier mobilities and lifetimes in organolead trihalide perovskites, *Adv. Mater.* **26**, 1584 (2014).
- [8] G. Giorgi and K. Yamashita, Organic–inorganic halide perovskites: An ambipolar class of materials with enhanced photovoltaic performances, *J. Mater. Chem. A* **3**, 8981 (2015).
- [9] H. Zhou, Q. Chen, G. Li, S. Luo, T.-B. Song, H.-S. Duan, Z. Hong, J. You, Y. Liu, and Y. Yang, Interface engineering of highly efficient perovskite solar cells, *Science* **345**, 542 (2014).
- [10] A. Walsh, Principles of chemical bonding and band gap engineering in hybrid organic–inorganic halide perovskites, *J. Phys. Chem. C* **119**, 5755 (2015).
- [11] B. Dieny, Giant magnetoresistance in spin-valve multilayers, *J. Magn. Magn. Mater.* **136**, 335 (1994).
- [12] Z. H. Xiong, D. Wu, Z. Valy Vardeny, and J. Shi, Giant magnetoresistance in organic spin-valves, *Nature* **427**, 821 (2004).
- [13] N. J. Harmon and M. E. Flatté, Spin-flip Induced Magnetoresistance in Positionally Disordered Organic Solids, *Phys. Rev. Lett.* **108**, 186602 (2012).
- [14] K. I. Kobayashi, T. Kimura, H. Sawada, K. Terakura, and Y. Tokura, Room-temperature magnetoresistance in an oxide material with an ordered double-perovskite structure, *Nature* **395**, 677 (1998).
- [15] M. M. Parish and P. B. Littlewood, Non-saturating magnetoresistance in heavily disordered semiconductors, *Nature* **426**, 162 (2003).
- [16] C. Zhang, D. Sun, C. X. Sheng, Y. X. Zhai, K. Mielczarek, A. Zakhidov, and Z. V. Vardeny, Magnetic field effects in hybrid perovskite devices, *Nat. Phys.* **11**, 427 (2015).
- [17] F. J. Wang, H. Bässler, and Z. Valy Vardeny, Magnetic Field Effects in  $\pi$ -Conjugated Polymer-Fullerene Blends: Evidence for Multiple Components, *Phys. Rev. Lett.* **101**, 236805 (2008).
- [18] T. D. Nguyen, Y. Sheng, J. Rybicki, G. Veeraraghavan, and M. Wohlgenannt, Magnetoresistance in  $\pi$ -conjugated organic sandwich devices with varying hyperfine and spin–orbit coupling strengths, and varying dopant concentrations, *J. Mater. Chem.* **17**, 1995 (2007).
- [19] V. N. Prigodin, J. D. Bergeson, D. M. Lincoln, and A. J. Epstein, Anomalous room temperature magnetoresistance in organic semiconductors, *Synth. Met.* **156**, 757 (2006).
- [20] K. Tanaka, T. Takahashi, T. Ban, T. Kondo, K. Uchida, and N. Miura, Comparative study on the excitons in lead-halide-based perovskite-type crystals  $CH_3NH_3PbBr_3$   $CH_3NH_3PbI_3$ , *Solid State Commun.* **127**, 619 (2003).
- [21] D. Niesner, M. Hauck, S. Shrestha, I. Levchuk, G. J. Matt, A. Osvet, M. Batentschuk, C. Brabec, H. B. Weber, and T. Fauster, Structural fluctuations cause spin-split states in tetragonal  $(CH_3NH_3)PbI_3$  as evidenced by the circular photogalvanic effect, *Proc. Natl. Acad. Sci. U.S.A.* **115**, 9509 (2018).
- [22] M. Kim, J. Im, A. J. Freeman, J. Ihm, and H. Jin, Switchable  $S = 1/2$  and  $J = 1/2$  rashba bands in ferroelectric halide perovskites, *Proc. Natl. Acad. Sci. U.S.A.* **111**, 6900 (2014).
- [23] J. Li and P. M. Haney, Optical spintronics in organic-inorganic perovskite photovoltaics, *Phys. Rev. B* **93**, 155432 (2016).

- [24] B. Bandyopadhyay, H. Luitel, S. Sil, J. Dhar, M. Chakrabarti, P. Nath, P. P. Ray, and D. Sanyal, NMR study of defect-induced magnetism in methylammonium lead iodide perovskite, *Phys. Rev. B* **101**, 094417 (2020).
- [25] Y. Yang, S. Feng, Z. Li, T. Li, Y. Xiong, L. Cao, and X. Gao, Unexpected outstanding room temperature spin transport verified in organic–inorganic hybrid perovskite film, *J. Phys. Chem. Lett.* **10**, 4422 (2019).
- [26] J. Wang, C. Zhang, H. Liu, X. Liu, H. Guo, D. Sun, and Z. V. Vardeny, Tunable spin characteristic properties in spin valve devices based on hybrid organic–inorganic perovskites, *Adv. Mater.* **31**, 1904059 (2019).
- [27] F. Li, J. Ding, W. Yu, X. Guan, P. Wang, D. Wu, and T. Wu, Light-enhanced spin diffusion in hybrid perovskite thin films and single crystals, *ACS Appl. Mater. Interfaces* **12**, 3205 (2020).
- [28] B. Náfrádi, P. Szirmai, M. Spina, H. Lee, O. V. Yazyev, A. Arakcheeva, D. Chernyshov, M. Gibert, L. Forró, and E. Horváth, Optically switched magnetism in photovoltaic perovskite  $\text{CH}_3\text{NH}_3(\text{Mn}:\text{Pb})\text{I}_3$ , *Nat. Commun.* **7**, 13406 (2016).
- [29] D. Giovanni, W. K. Chong, H. A. Dewi, K. Thirumal, I. Neogi, R. Ramesh, S. Mhaisalkar, N. Mathews, and T. C. Sum, Tunable room-temperature spin-selective optical Stark effect in solution-processed layered halide perovskites, *Sci. Adv.* **2**, e1600477 (2016).
- [30] Y. Li, S. He, X. Luo, X. Lu, and K. Wu, Strong spin-selective optical stark effect in lead halide perovskite quantum dots, *J. Phys. Chem. Lett.* **11**, 3594 (2020).
- [31] D. Niesner, M. Wilhelm, I. Levchuk, A. Osvet, S. Shrestha, M. Batentschuk, C. Brabec, and T. Fauster, Giant Rashba Splitting in  $\text{CH}_3\text{NH}_3\text{PbBr}_3$  Organic-Inorganic Perovskite, *Phys. Rev. Lett.* **117**, 126401 (2016).
- [32] M. Kepenekian, R. Robles, C. Katan, D. Saporì, L. Pedesseau, and J. Even, Rashba and Dresselhaus effects in hybrid organic–inorganic perovskites: From basics to devices, *ACS Nano* **9**, 11557 (2015).
- [33] Q. Xu, E. Liu, S. Qin, S. Shi, K. Shen, M. Xu, Y. Zhai, and S. Dong, Spin transport in  $\text{CH}_3\text{NH}_3\text{PbI}_3$ , *J. Phys. D: Appl. Phys.* **47**, 405002 (2014).
- [34] K. Zhu, J. Chen, Q. Fan, L. Wang, and Q. Xu, Magnetoresistance of  $(\text{CH}_3\text{NH}_3)\text{PbI}_3$ -coated  $\text{La}_{0.67}\text{Sr}_{0.33}\text{MnO}_3$  granular composites, *IEEE Trans. Magn.* **51**, 1 (2015).
- [35] N.-G. Park, Methodologies for high efficiency perovskite solar cells, *Nano Converg.* **3**, 15 (2016).
- [36] See Supplemental Material at <http://link.aps.org/supplemental/10.1103/PhysRevApplied.14.064018> for experimental details and Figs. S1–S6.
- [37] R. Comin, G. Walters, E. S. Thibau, O. Voznyy, Z.-H. Lu, and E. H. Sargent, Structural, optical, and electronic studies of wide-bandgap lead halide perovskites, *J. Mater. Chem. C* **3**, 8839 (2015).
- [38] D. Cui, Z. Yang, D. Yang, X. Ren, Y. Liu, Q. Wei, H. Fan, J. Zeng, and S. Liu, Color-tuned perovskite films prepared for efficient solar cell applications, *J. Phys. Chem. C* **120**, 42 (2016).
- [39] P. Odenthal, W. Talmadge, N. Gundlach, R. Wang, C. Zhang, D. Sun, Z.-G. Yu, Z. Valy Vardeny, and Y. S. Li, Spin-polarized exciton quantum beating in hybrid organic–inorganic perovskites, *Nat. Phys.* **13**, 894 (2017).
- [40] R. H. Friend, R. W. Gymer, A. B. Holmes, J. H. Burroughes, R. N. Marks, C. Taliani, D. D. C. Bradley, D. A. D. Santos, J. L. Brédas, M. Lögdlund *et al.*, Electroluminescence in conjugated polymers, *Nature* **397**, 121 (1999).
- [41] J. S. Wilson, A. S. Dhoot, A. J. A. B. Seeley, M. S. Khan, A. Köhler, and R. H. Friend, Spin-dependent exciton formation in  $\pi$ -conjugated compounds, *Nature* **413**, 828 (2001).
- [42] Z. G. Yu, Spin-orbit coupling and its effects in organic solids, *Phys. Rev. B* **85**, 115201 (2012).
- [43] B. Hu, L. Yan, and M. Shao, Magnetic-field effects in organic semiconducting materials and devices, *Adv. Mater.* **21**, 1500 (2009).
- [44] B. R. Gautam, T. D. Nguyen, E. Ehrenfreund, and Z. Valy Vardeny, Magnetic field effect on excited-state spectroscopies of  $\pi$ -conjugated polymer films, *Phys. Rev. B* **85**, 205207 (2012).
- [45] J. C. Blancon, A. V. Stier, H. Tsai, W. Nie, C. C. Stoumpos, B. Traoré, L. Pedesseau, M. Kepenekian, F. Katsutani, G. T. Noe *et al.*, Scaling law for excitons in 2D perovskite quantum wells, *Nat. Commun.* **9**, 2254 (2018).
- [46] E. Ehrenfreund and Z. V. Vardeny, Effects of magnetic field on conductance and electroluminescence in organic devices, *Isr. J. Chem.* **52**, 552 (2012).
- [47] J. Even, L. Pedesseau, J.-M. Jancu, and C. Katan, Importance of spin–orbit coupling in hybrid organic/inorganic perovskites for photovoltaic applications, *J. Phys. Chem. Lett.* **4**, 2999 (2013).
- [48] A. H. Devir-Wolfman, B. Khachatryan, B. R. Gautam, L. Tzabary, A. Keren, N. Tessler, Z. V. Vardeny, and E. Ehrenfreund, Short-lived charge-transfer excitons in organic photovoltaic cells studied by high-field magneto-photocurrent, *Nat. Commun.* **5**, 4529 (2014).
- [49] A. Amat, E. Mosconi, E. Ronca, C. Quarti, P. Umari, M. K. Nazeeruddin, M. Grätzel, and F. De Angelis, Cation-induced band-gap tuning in organohalide perovskites: Interplay of spin–orbit coupling and octahedra tilting, *Nano Lett.* **14**, 3608 (2014).
- [50] S. Yang, E. Vetter, T. Wang, A. Amassian, and D. Sun, Observation of long spin lifetime in  $\text{MAPbBr}_3$  single crystals at room temperature, *J. Phys. Mater.* **3**, 015012 (2020).
- [51] D. Giovanni, H. Ma, J. Chua, M. Grätzel, R. Ramesh, S. Mhaisalkar, N. Mathews, and T. C. Sum, Highly spin-polarized carrier dynamics and ultralarge photoinduced magnetization in  $\text{CH}_3\text{NH}_3\text{PbI}_3$  perovskite thin films, *Nano Lett.* **15**, 1553 (2015).
- [52] Z.-G. Yu and Y. S. Li, Unraveling the spin relaxation mechanism in hybrid organic–inorganic perovskites, *J. Phys. Chem. C* **123**, 14701 (2019).